Analysis of Spectrally Efficient Random FM Radar Waveforms

Jonathan W. Owen, Christian C. Jones, Patrick M. McCormick, David G. Felton,
Matthew B. Heintzelman, Jennifer E. Quirk, Shannon D. Blunt
Radar Systems Laboratory, University of Kansas

***Abstract*— Random FM (RFM) waveforms have recently been demonstrated to achieve desirable power spectrum characteristics commensurate with low pulse compression sidelobes. Separately, the limitations of correlation-based processing were assessed by determining the optimum null-constrained power spectrum that minimizes correlation sidelobe levels. RFM waveforms that are spectrally shaped to approximate the optimum spectrum consequently exhibit near-optimum range sidelobe levels given sufficient degrees of freedom. In this context, an RFM design variant denoted Spectrally Weighted Frequency Template Error (SWiFTE) is evaluated relative to other modern designs. Performance analysis is assessed in terms of spectral containment, correlation sidelobe levels, and optimization convergence speeds.**

Index Terms*—*waveform diversity, pulse compression, random frequency modulation (RFM), spectrum sharing

I. Introduction

Growing RF congestion represents a transition from the era of noise-limited legacy radar to pervasive interference-limited operation. Nonrepeating random FM (RFM) waveforms [1] provide inherent design freedom and flexibility that make them readily amenable to spectrum shaping, which can incorporate dynamic notches to mitigate interference with proximate RF users [2,3]. Moreover, their FM structure is compatible with high-power transmitters due to a constant amplitude envelope and continuous phase attributes. Because RFM waveforms possess a thumbtack ambiguity function (recalling that energy is conserved), individual pulses cannot attain quite the degree of low range sidelobe performance as an optimized chirp-like structure for a set time-bandwidth product [4]. However, slow-time combining across P unique RFM waveforms realizes $\sim 10\log_{10}(P)$ incoherent averaging suppression of sidelobes [1].

The power spectral density (PSD) and autocorrelation are a Fourier transform pair; therefore, waveforms designed to conform to a PSD template can be directly optimized for both autocorrelation and spectral properties. To gain insight about the behavior of notched power spectra, [5] determined the global optimum PSD that minimizes integrated sidelobe level (ISL) or peak sidelobe level (PSL) with spectral null constraints for a given autocorrelation mainlobe resolution. As the autocorrelation mainlobe width is increased, the sidelobe floor is correspondingly reduced, establishing a fundamental trade-space between range resolution and correlation error. However, the optimum PSD template cannot be precisely attained with time-limited waveforms.

A variety of spectrally notched RFM waveforms have been developed (e.g. [6-11]) but have not been commonly evaluated relative to standard radar performance metrics. The tradeoff between optimality, convergence speed, and computational cost is critical when considering real-time implementation. For instance, pseudo-random optimized FM (PRO-FM) waveforms combined with supplementary spectral nulling were found to suitably meet the criterion for real-time radar spectrum sharing [3]. Even so, alternative strategies merit evaluation.

Here the frequency template-based waveform designs explored in [6-11] are analyzed when designed according to the null-constrained spectrum template for ISL minimization from [5]. An alternative waveform scheme denoted Spectrally Weighted Frequency Template Error (SWiFTE) is proposed that exhibits well-rounded metric performance. Resultant waveforms are examined in terms of percent energy spectral containment, ISL, PSL, and optimization convergence speeds.

II. Waveform Designs & Metric Analysis

The waveform designs from [6-11] are evaluated herein, including PRO-FM [6, 7], frequency template error (FTE) [8], logarithmic-domain FTE (Log-FTE) [8], and temporal template error (TTE) [9, 10]. The zero-order reconstruction of waveforms (ZOROW) algorithm is a waveform *modifier* that rapidly deepens spectral notches, though the desired spectrum shape may be adversely altered [11]. The SWIFTE objective function is described, which modifies FTE with a weighting to emphasize error in user-specified spectral regions.

Each discretized waveform design requires a user-defined desired power spectrum $\mathbf{d}_{\mathrm{f}}$. For consistent comparison, all waveform designs herein use the optimum spectrum $\hat{\mathbf{d}}_{\mathrm{f}}$ from [5] that minimizes autocorrelation sidelobe levels for a specified mainlobe resolution while maintaining spectral null constraints. This template $\hat{\mathbf{d}}_{\mathrm{f}}$ is found from the convex objective function

$$\begin{aligned} &\min_{\mathbf{d}_{\mathrm{f}}} \|\mathbf{e} - \mathbf{A}^H \mathbf{d}_{\mathrm{f}}\|_p^p \\ &\text{s.t. } d_{\mathrm{f},m} \le \gamma_m \quad \text{for } m \in \Lambda \\ &\qquad 0 \le d_{\mathrm{f},m} \quad \text{for } m = 0, 1, \ldots, M-1 \end{aligned} \tag{1}$$

where $m = 0, 1, \ldots, M-1$ indicates discrete frequency, $\mathbf{e}$ is the desired autocorrelation response (a unit impulse), $\mathbf{A}$ is the $M \times M$ discrete Fourier transform matrix, γ_m is the constrained maximum value for the associated $d_{\mathrm{f},m}$ when m is in the subset Λ (i.e. null constraints), and selection of $p = 2$ minimizes ISL whereas $p \to \infty$ minimizes PSL. The operator $\|\cdot\|_p$ is the vector p-norm, with $\|\cdot\|_p^p$ exponentiated. Different degrees of mainlobe resolution are achievable by replacing $\bar{M}$ rows of $\mathbf{A}$ (corresponding to autocorrelation mainlobe roll-off) with zeros. Here $\gamma_m = 10^{-3}$ (or 30 dB depth), $p = 2$, and $\bar{M} = 2$ are used.

This work was supported by the Office of Naval Research under Contract #N00014-23-C-1053. DISTRIBUTION STATEMENT A. Approved for public release.

The optimization routines for waveform designs [6-11] are shown in Table I and associated gradients are in Table II. Relevant variables from Tables I & II are described in Table III. Note that PRO-FM does not have an explicit objective function and instead performs Q alternating time-frequency projections. TTE minimizes an objective function but requires a final constant envelope projection and truncation upon convergence. All function minimizations are performed with limited-memory Broyden-Fletcher-Goldfarb-Shanno (L-BFGS) [12] using the "minf_lbfgs" function from the TensorLab toolkit [13]. Operators include: $\angle\{\bullet\}$ extracts the phase argument, $\odot$ is the Hadamard product, $\log_b(\mathrm{x})$ takes the base-b logarithm, and $\mathrm{sinc}(\mathrm{x}) = \sin(\pi\mathrm{x})/\pi\mathrm{x}$ for $\mathrm{x} \neq 0$; $\mathrm{sinc}(\mathrm{x}) = 1$ otherwise.

The temporal power envelopes are held constant as $\mathbf{u} = \mathbf{1}_{N\times 1}$ to maintain FM attributes. In [14] it was noted that the Nyquist theorem is dual, so the number of evaluated frequency samples must be $M \geq 2N-1$. For this analysis, $M = 2N-1$ is selected.

The FTE, Log-FTE, SWiFTE, and ZOROW designs incorporate "quasi-basis" matrix $\mathbf{B}$ into the signal exponent, allowing for phase structure implementation [15, 16] including polyphase coded FM (PCFM), higher-order PCFM (HO-PCFM), and constant envelope orthogonal frequency division multiplexing (CE-OFDM). Here the quasi-basis is set to an identity matrix $\mathbf{B} = \mathbf{I}$ to directly optimize phase, otherwise known as angle modulation since spectral containment implicitly limits the amount of sample-wise phase change [17]. The PRO-FM and TTE designs cannot be optimized with a quasi-basis due to projection stages. The optimized parameters $\mathbf{x}$ are cast into $\tilde{\mathbf{x}} = \pi\cos(\mathbf{x})$ to implicitly constrain $\tilde{\mathbf{x}} \in [-\pi, \pi)$.

The emphasis vector $\mathbf{w}_{\mathrm{error}}$ applied in the SWiFTE design may be arbitrarily chosen, although the selected option is

$$\mathbf{w}_{\mathrm{error}} = \begin{cases} \mathbf{d}_{\mathrm{f}}{}^{-\alpha} \text{ for } m \notin \Lambda \\ \mathbf{d}_{\mathrm{f}}{}^{-1} \text{ for } m \in \Lambda \end{cases} \tag{2}$$

where Λ are frequency regions containing spectral nulls, and α otherwise allows for tuning to minimize error in high-power or low-power spectral regions. It is recommended to maintain $\alpha \in [0,1]$ for numerical stability during optimization. Unless otherwise specified, $\alpha = 1$ for remaining analysis. To reiterate, here $\mathbf{d}_{\mathrm{f}}$ is fixed to be the optimum $\hat{\mathbf{d}}_{\mathrm{f}}$ from (1).

Table I: Optimization Routines & Objective Functions

PRO-FM	$\dot{\mathbf{s}}^{(q+1)} = \tilde{\mathbf{A}}^H\{\mathbf{d}_{\mathrm{f}}^{1/2} \odot \exp(j\angle\tilde{\mathbf{A}}\mathbf{s}^{(q)})\}$ $\mathbf{s}^{(q+1)} = \mathbf{u}^{1/2} \odot \exp(j\angle\dot{\mathbf{s}}^{(q+1)})$
FTE	$\min_{\mathbf{x}} \left\|(\tilde{\mathbf{A}}\mathbf{s}) \odot (\tilde{\mathbf{A}}\mathbf{s})^* - \mathbf{d}_{\mathrm{f}}\right\|_2^2$ where $\mathbf{s} = e^{j\pi\mathbf{B}\cos(\mathbf{x})}$
Log-FTE	$\min_{\mathbf{x}} \left\|\log_b[(\tilde{\mathbf{A}}\mathbf{s}) \odot (\tilde{\mathbf{A}}\mathbf{s})^*] - \log_b[\mathbf{d}_{\mathrm{f}}]\right\|_2^2$ where $\mathbf{s} = e^{j\pi\mathbf{B}\cos(\mathbf{x})}$
SWiFTE	$\min_{\mathbf{x}} \left\|\mathbf{w}_{\mathrm{error}} \odot [(\tilde{\mathbf{A}}\mathbf{s}) \odot (\tilde{\mathbf{A}}\mathbf{s})^* - \mathbf{d}_{\mathrm{f}}]\right\|_2^2$ where $\mathbf{s} = e^{j\pi\mathbf{B}\cos(\mathbf{x})}$
TTE	$\min_{\boldsymbol{\phi}_{\mathrm{f}}} \|\bar{\mathbf{s}} \odot \bar{\mathbf{s}}^* - [\mathbf{u}^T\ \mathbf{0}_{1\times N}]^T\|_2^2$ where $\bar{\mathbf{s}} = \mathbf{A}^H(\mathbf{d}_{\mathrm{f}}^{1/2} \odot e^{j\boldsymbol{\phi}_{\mathrm{f}}})$ Final Projection: $\mathbf{s} = \mathbf{u}^{1/2} \odot e^{j\angle\{\tilde{\mathbf{A}}^H(\mathbf{d}_{\mathrm{f}}^{1/2} \odot e^{j\boldsymbol{\phi}_{\mathrm{f}}})\}}$
ZOROW	$\min_{\mathbf{x}} \left\|\mathbf{w}_\Lambda \odot \left(\mathbf{T}^T \mathrm{sinc}\left(\frac{\mathbf{m} - \lfloor M/2 \rfloor}{M}\right) \odot \tilde{\mathbf{A}}\mathbf{s}\right)\right\|_2^2$ where $\mathbf{s} = e^{j\pi\mathbf{B}\cos(\mathbf{x})}$

Table II: Objective Function Gradients

FTE	$\nabla_{\mathbf{x}} J = -4\pi\sin(\mathbf{x}) \odot$ $\mathbf{B}^T\Im\left\{\mathbf{s}^* \odot \left[\tilde{\mathbf{A}}^H\left((\tilde{\mathbf{A}}\mathbf{s}) \odot (\tilde{\mathbf{A}}\mathbf{s})^* - \mathbf{d}_{\mathrm{f}}\right) \odot \tilde{\mathbf{A}}\mathbf{s}\right]\right\}$
Log-FTE	$\nabla_{\mathbf{x}} J = \frac{-4\pi}{\ln(b)}\sin(\mathbf{x}) \odot$ $\mathbf{B}^T\Im\left\{\mathbf{s}^* \odot \left[\tilde{\mathbf{A}}^H\left(\log_b\left((\tilde{\mathbf{A}}\mathbf{s}) \odot (\tilde{\mathbf{A}}\mathbf{s})^*\right) - \log_b(\mathbf{d}_{\mathrm{f}})\right) \oslash (\tilde{\mathbf{A}}\mathbf{s})^*\right]\right\}$
SWiFTE	$\nabla_{\mathbf{x}} J = -4\pi\sin(\mathbf{x}) \odot \mathbf{B}^T\Im\left\{\mathbf{s}^* \odot \left[\tilde{\mathbf{A}}^H\left(\mathbf{w}_{\mathrm{error}} \odot \mathbf{w}_{\mathrm{error}} \odot \left((\tilde{\mathbf{A}}\mathbf{s}) \odot (\tilde{\mathbf{A}}\mathbf{s})^* - \mathbf{d}_{\mathrm{f}}\right) \odot \tilde{\mathbf{A}}\mathbf{s}\right)\right]\right\}$
TTE	$\nabla_{\boldsymbol{\phi}_{\mathrm{f}}} J = 4\,\Im\left\{(\mathbf{d}_{\mathrm{f}}^{1/2} \odot e^{j\boldsymbol{\phi}_{\mathrm{f}}})^* \odot \tilde{\mathbf{A}}(\bar{\mathbf{s}} \odot (\bar{\mathbf{s}} \odot \bar{\mathbf{s}}^* - [\mathbf{u}^T\ \mathbf{0}_{1\times N}]^T))\right\}$
ZOROW	$\nabla_{\mathbf{x}} J = -4\pi\sin(\mathbf{x}) \odot$ $\mathbf{B}^T\Im\left\{\tilde{\mathbf{A}}^H\left(\mathbf{w}_\Lambda \odot \mathbf{T}^T \mathrm{sinc}\left(\frac{\mathbf{m} - \lfloor M/2 \rfloor}{M}\right) \odot \tilde{\mathbf{A}}\mathbf{s}\right)\right\}$

In Table II, $\oslash$ performs an element-wise division, $\Im$ extracts the imaginary values, and $\lfloor\cdot\rfloor$ is the floor operator.

Table III: Waveform Parameters

Parameter	Dimensions	Description
$\mathbf{s}$	$N \times 1$	Radar waveform
$\dot{\mathbf{s}}$	$M \times 1$	Intermediate variable (PRO-FM)
$\bar{\mathbf{s}}$	$M \times 1$	Intermediate variable (TTE)
$\mathbf{u}$	$N \times 1$	Desired temporal power envelope template (typically constant)
$\mathbf{d}_{\mathrm{f}}$	$M \times 1$	Desired frequency power spectrum template
$\mathbf{A}$	$M \times M$	Discrete Fourier transform matrix
$\tilde{\mathbf{A}}$	$M \times N$	Truncated discrete Fourier transform matrix
$\mathbf{T}$	$M \times M$	FFT-shift transformation matrix ($\mathbf{T}^T$ performs the inverse shift)
m	1×1	The m^{th} discrete frequency index, where $m = 0, 1, \ldots, M-1$
$\mathbf{m}$	$M \times 1$	Set of discrete frequency indices, $\mathbf{m} = [0 \quad 1 \quad \cdots \quad M-1]$
$\boldsymbol{\phi}_{\mathrm{f}}$	$M \times 1$	Optimized parameters (see Table I); TTE spectrum phasor
$\mathbf{x}$	$K \times 1$	Optimized parameters (see Table I); then cast to $\tilde{\mathbf{x}} = \pi\cos(\mathbf{x}) \in [-\pi, \pi)$
$\mathbf{B}$	$N \times K$	Arbitrary quasi-basis function matrix, e.g. Identity, PCFM, HO-PCFM, CE-OFDM
$\mathbf{w}_\Lambda$	$M \times 1$	Spectrum notch mask $\mathbf{w}_\Lambda = \begin{cases} 0 & \text{for } m \notin \Lambda \\ 1 & \text{for } m \in \Lambda \end{cases}$
$\mathbf{w}_{\mathrm{error}}$	$M \times 1$	Error emphasis weights $\mathbf{w}_{\mathrm{error}} = \begin{cases} \mathbf{d}_{\mathrm{f}}{}^{-\alpha} \text{ for } m \notin \Lambda \\ \mathbf{d}_{\mathrm{f}}{}^{-1} \text{ for } m \in \Lambda \end{cases}$

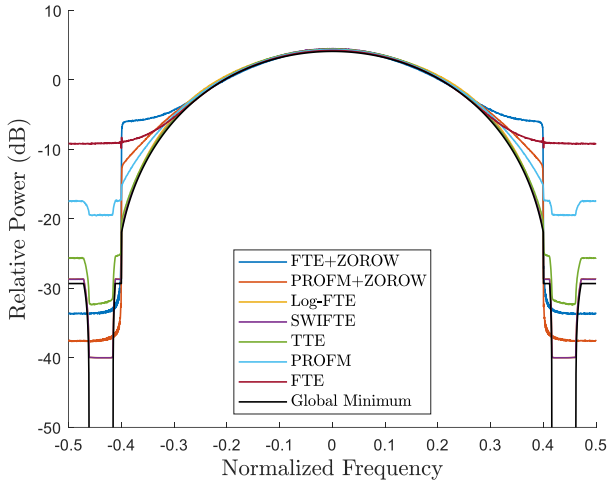

Fig. 1: Mean power spectra $\frac{1}{P}\sum_{\forall p}\left|\tilde{\mathbf{A}}\mathbf{s}_p\right|^2$ (indicating spectral containment) of waveform types; for $P = 10{,}000$ pulses, $N = 1000$ samples.

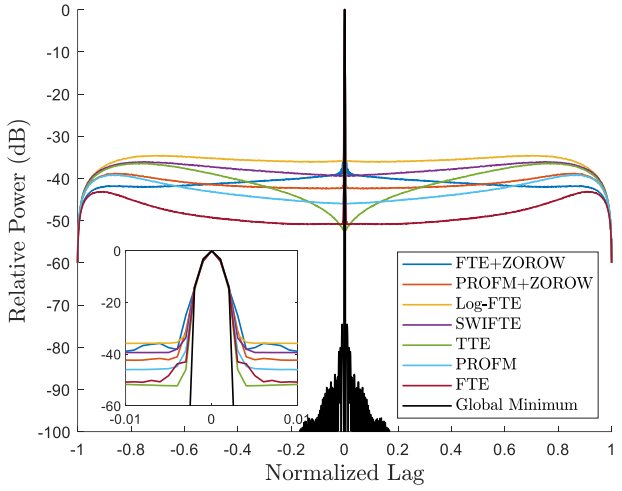

Fig. 2: RMS autocorrelation $\sqrt{\frac{1}{P}\sum_{\forall p}\left|\mathbf{r}_p\right|^2}$ (indicating per-pulse range sidelobe performance) of waveform types; for $P = 10{,}000$ pulses, $N = 1000$ samples.

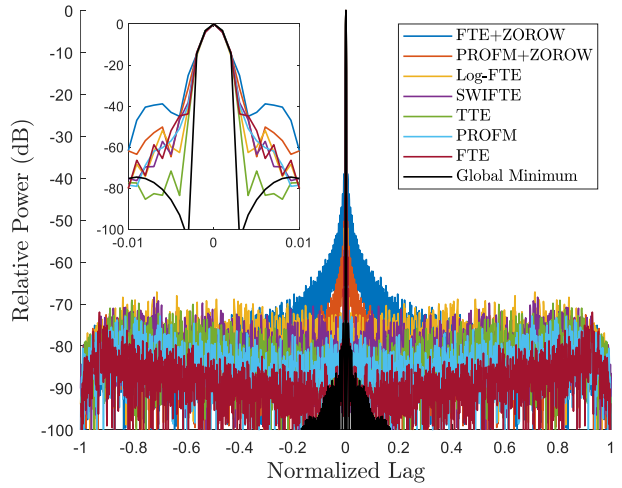

Fig. 3: Mean autocorrelation $\frac{1}{P}\sum_{\forall p}\mathbf{r}_p$ (indicating combined range sidelobe performance) of waveform types; for $P = 10{,}000$ pulses, $N = 1000$ samples.

For the designated waveform types, $P = 10{,}000$ pulses with $N = 1000$ samples each are formed. All waveform optimizations are performed until full algorithm convergence. Because both Log-FTE and SWiFTE increase error emphasis in deep spectral notch regions (which can cause overfitting), the desired spectrum template is loaded as $\mathbf{d}_\mathrm{f} = \hat{\mathbf{d}}_\mathrm{f} + \delta\mathbf{1}_{N\times 1}$ where $\delta = 10^{-4}$ slightly deemphasizes the notched regions Λ. The ZOROW modifier is applied only to waveforms that innately exhibit less spectral containment, specifically FTE and PRO-FM. The mean power spectra of optimized waveform sets are shown in Fig. 1, while the root-mean-squared (RMS) and mean autocorrelations are illustrated in Figs. 2 and 3, respectively. The number of frequency samples is chosen as $M = 2N - 1$, which conveniently is the signal autocorrelation length. The global minimum PSD $\hat{\mathbf{d}}_\mathrm{f}$ or autocorrelation $\hat{\mathbf{d}} = \mathbf{A}^H\hat{\mathbf{d}}_\mathrm{f}$ is illustrated in Figs. 1-3 for comparison but cannot be precisely achieved with time-finite waveforms.

It is well known that a deterministic signal autocorrelation $\mathbf{r} = \mathbf{s} \star \mathbf{s}$ and power spectrum $\mathbf{r}_\mathrm{f} = \left|\tilde{\mathbf{A}}\mathbf{s}\right|^2$ are Fourier transform pairs, such that $\mathbf{r} = \mathbf{A}^H\left|\tilde{\mathbf{A}}\mathbf{s}\right|^2$. Due to linearity of the Fourier transform operator, a pair likewise exists between the mean autocorrelation and the mean power spectrum across P pulses:

$$\frac{1}{P}\sum_{\forall p}\mathbf{r}_p = \mathbf{A}^H\left(\frac{1}{P}\sum_{\forall p}\left|\tilde{\mathbf{A}}\mathbf{s}_p\right|^2\right). \tag{3}$$

Noting that each waveform spectrum is shaped to the optimum template $\hat{\mathbf{d}}_\mathrm{f}$, then waveform sets that adhere closest to $\hat{\mathbf{d}}_\mathrm{f}$ in the mean power spectrum will implicitly exhibit minimized autocorrelation sidelobes after coherent integration. The RMS autocorrelation indicates typical per-pulse sidelobe performance, expressed as $\sqrt{\frac{1}{P}\sum_{\forall p}\left|\mathbf{r}_p\right|^2}$.

Metrics applied to the waveform sets include percent energy spectral containment, ISL, PSL, and optimization convergence speeds. Spectral containment is measured by the percentage of signal energy remaining in the spectral null regions. The notch locations are indicated by $\mathbf{w}_\Lambda$ as defined in Table III. The percent energy is defined as

$$\%\ \text{Energy} = \frac{\sum_{\forall p}\mathbf{w}_\Lambda^T\left|\tilde{\mathbf{A}}\mathbf{s}_p\right|^2}{\sum_{\forall p}\mathbf{1}_{M\times 1}^T\left|\tilde{\mathbf{A}}\mathbf{s}_p\right|^2}. \tag{4}$$

The autocorrelation sidelobes levels are measured in terms of ISL and PSL, applied to both the RMS autocorrelation and the mean autocorrelation (with either represented by $\tilde{\mathbf{r}}$). The integrated sidelobe level metric is defined as

$$\text{ISL} = \frac{\left\|\mathbf{w}_\mathrm{sl}\odot\tilde{\mathbf{r}}\right\|_2^2}{\mathbf{1}_{M\times 1}^T\mathbf{w}_\mathrm{sl}}, \tag{5}$$

where $\mathbf{w}_\mathrm{sl}$ selects the autocorrelation sidelobes with 1's (and removes the autocorrelation mainlobe with 0's). The peak sidelobe level metric is similarly represented as

$$\text{PSL} = \left\|\mathbf{w}_\mathrm{sl}\odot\tilde{\mathbf{r}}\right\|_\infty^2, \tag{6}$$

where $\|\cdot\|_\infty$ determines the maximum value.

Both Log-FTE and SWiFTE achieve the specified spectral containment, while TTE is 3.8 dB shallower. The typical containment achieved by FTE and PRO-FM are orders of magnitude shallower by comparison, but subsequent application of ZOROW then realizes similar performance. However, the spectral shape after ZOROW demonstrates a rectangular mask (due to less rounded edges) that implies a sinc structure in the mean autocorrelation sidelobes, seen in Fig. 3.

Table IV: Waveform Performance Metrics (Contiguous Bandwidth)

	% Energy	RMS ISL (dB)	RMS PSL (dB)	Mean ISL (dB)	Mean PSL (dB)	Iterations
FTE+ZOROW	$1.12 \cdot 10^{-4}$	–41.05	–35.84	–61.59	–38.90	-
PRO-FM+ZOROW	$4.20 \cdot 10^{-5}$	–41.05	–38.81	–73.70	–50.17	-
Log-FTE	$1.41 \cdot 10^{-4}$	–35.75	–34.55	–74.70	–51.86	455
SWiFTE	$1.40 \cdot 10^{-4}$	–37.70	–36.05	–77.10	–57.18	353
TTE	$3.39 \cdot 10^{-4}$	–39.42	–36.40	–79.53	–69.08	159
PRO-FM	$2.95 \cdot 10^{-3}$	–42.40	–39.12	–79.88	–56.91	85
FTE	$2.45 \cdot 10^{-2}$	–47.50	–43.12	–79.68	–51.97	97

The RMS autocorrelation metrics exemplify the expected per-pulse performance. FTE and PRO-FM perform best for both RMS sidelobe metrics, which is anticipated due to shallower spectral containment. Upon applying ZOROW, they achieve similar ISL, but FTE exhibits 3 dB higher PSL than PRO-FM. The innately contained waveforms - Log-FTE, SWiFTE, and TTE - have quite different RMS autocorrelations despite comparable power spectra. Variations are due to the degree of spectrum match. Log-FTE exhibits the uppermost per-pulse sidelobe levels whereas SWiFTE achieves 2.5 dB less. Similarly, TTE and SWiFTE have nearly identical RMS PSL, but TTE achieves lower RMS ISL (due to slightly shallower spectral containment).

The mean autocorrelation metrics are relatively similar to the RMS metrics; however, incoherent sidelobe integration unveils structure in relation to the mean power spectrum. It was previously mentioned that a sinc structure appears in the mean autocorrelation when ZOROW is applied due to the ensuant rectangular mean spectrum shape, increasing both PSL and ISL. The zoomed inset of Fig. 3 shows mainlobe resolution broadening, where TTE is the narrowest of the batch. Log-FTE forms a slightly thinner mainlobe than SWiFTE, while PRO-FM and FTE are comparable. The peak sidelobe reduction of TTE over other methods (>12 dB) implies a closer match to the template $\hat{\mathbf{d}}_\mathrm{f}$. Again, TTE cannot be optimized with a quasi-basis.

Although distinct objective functions exist for each waveform type, the number of iterations prior to convergence provides practical insight. Because PRO-FM does not have an explicit objective function, it is instead evaluated according to the FTE metric. The waveform designs under consideration attempt to minimize an objective function J to match a desired spectrum template $\mathbf{d}_\mathrm{f}$. Consequently, the convergence speeds are dependent on the spectrum template and initialization. Here, the mean iterative cost function values are represented for those waveforms generated in Figs. 1-3, shown in Fig. 4. The L-BFGS method is considered fully converged when the objective function decreases by less than 0.01 dB between successive iterations. The number of iterations prior to convergence are summarized in Table IV. Notably, the PRO-FM algorithm rapidly converges before a shallow plateau (due to the rapid but inexact convergence of alternating projections [6, 7]), while Log-FTE and SWiFTE converge more steadily.

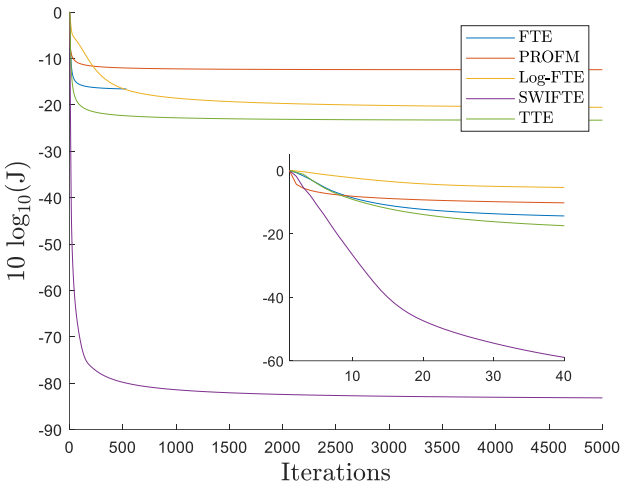

Fig. 4: Objective function value J versus iteration for respective waveform designs (see Table I). PRO-FM is evaluated with the FTE metric. Due to distinct objective functions, analysis is limited to relative convergence speeds.

Additional insight can be drawn by considering waveforms having a spectral notch in the center of the occupied bandwidth. Within the normalized frequency range of (–0.2, –0.1), an intentionally asymmetric null is introduced for metric comparison. The optimal template $\hat{\mathbf{d}}_\mathrm{f}$ is determined for a non-contiguous spectrum and the waveforms in Table I are optimized with the updated notch regions Λ. The mean power spectra of the optimized waveform sets are shown in Fig. 5, while the RMS and mean autocorrelations are illustrated in Figs. 6 and 7. The updated global minimum PSD $\hat{\mathbf{d}}_\mathrm{f}$ or autocorrelation $\hat{\mathbf{d}} = \mathbf{A}^H \hat{\mathbf{d}}_\mathrm{f}$ are illustrated in Figs. 5-7 for comparison but cannot be precisely achieved with time-limited waveforms. The optimum PSD $\hat{\mathbf{d}}_\mathrm{f}$ for various null locations is examined in [5], and the waveform analysis presented here is generalizable for other spectrum null regions.

When a central spectrum notch is present, the optimum integrated sidelobe levels are degraded as one would expect. The spectral containment exhibits performance akin to the contiguous spectrum case. The RMS PSL is higher for all cases, recalling that the template $\hat{\mathbf{d}}_\mathrm{f}$ is optimized for ISL here (not PSL). However, the RMS ISL performances are rather unchanged. The mean autocorrelations of the notched spectrum demonstrate near equivalent PSL performance for all waveforms, with only minor ISL performance deviations. In the mean, the optimum sidelobe levels are reached such that additional coherent integration would result in only minor improvement in the correlation tails.

Table V: Waveform Performance Metrics (Non-contiguous Bandwidth)

	% Energy	RMS ISL (dB)	RMS PSL (dB)	Mean ISL (dB)	Mean PSL (dB)	Iterations
FTE+ZOROW	$6.80 \cdot 10^{-4}$	-38.50	-29.63	-54.70	-30.83	-
PRO-FM+ZOROW	$2.89 \cdot 10^{-4}$	-39.36	-31.44	-56.69	-32.12	-
Log-FTE	$3.08 \cdot 10^{-4}$	-34.67	-27.87	-56.20	-28.96	494
SWiFTE	$2.80 \cdot 10^{-4}$	-36.27	-31.25	-58.55	-32.45	362
TTE	$9.15 \cdot 10^{-4}$	-38.33	-33.99	-59.33	-34.09	152
PRO-FM	$4.88 \cdot 10^{-3}$	-41.42	-33.60	-58.71	-33.94	79
FTE	$3.79 \cdot 10^{-2}$	-47.22	-36.02	-62.37	-36.18	99

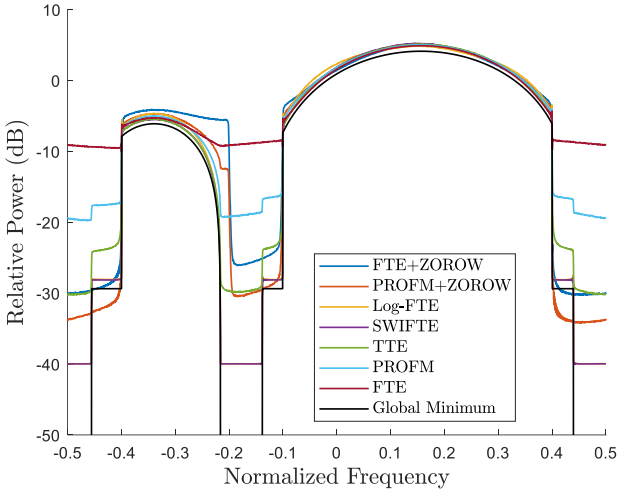

Fig. 5: Mean power spectra $\frac{1}{P}\sum_{\forall p}\left|\tilde{\mathbf{A}}\mathbf{s}_p\right|^2$ of waveform types; for $P = 10{,}000$ pulses, $N = 1000$ samples.

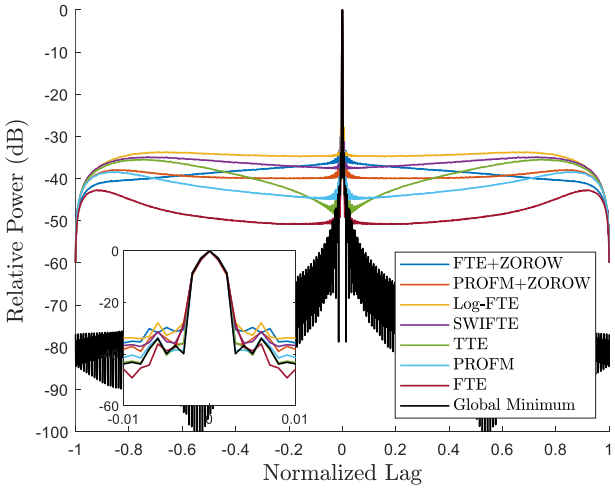

Fig. 6: RMS autocorrelation $\sqrt{\frac{1}{P}\sum_{\forall p}\left|\mathbf{r}_p\right|^2}$ of waveform types; for $P = 10{,}000$ pulses, $N = 1000$ samples.

III. Aspects of SWIFTE

With the SWiFTE waveform design now introduced, the error weighting vector $\mathbf{w}_{\text{error}}$ is tuned relative to the variable α. Recalling the weight definition in (2), α allows for tuning to minimize error in high-power or low-power spectral regions, with a recommended setting of $\alpha \in [0,1]$. The notched regions subsumed in Λ are maintained by the piecewise emphasis vector definition from (2).

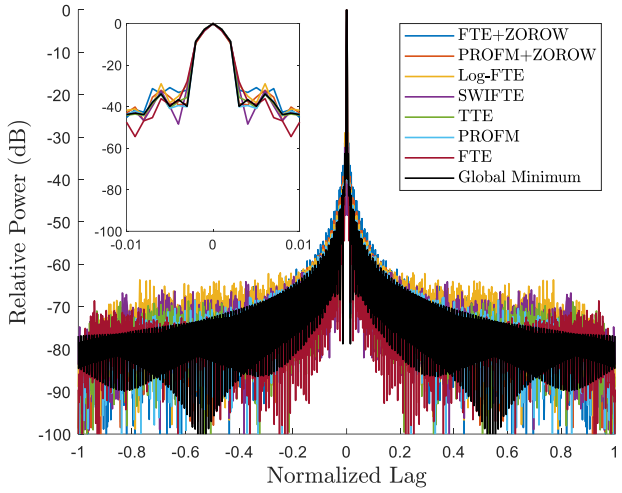

Fig. 7: Mean autocorrelation $\frac{1}{P}\sum_{\forall p}\mathbf{r}_p$ of waveform types; for $P = 10{,}000$ pulses, $N = 1000$ samples.

The SWiFTE waveforms are matched to the template $\mathbf{d}_{\text{f}} = \hat{\mathbf{d}}_{\text{f}} + \delta\mathbf{1}_{N\times 1}$ where $\delta = 10^{-4}$ for a contiguous power spectrum (as in Figs. 1-3). The tuning parameter is varied for $\alpha = 0.0, 0.25, 0.5, 0.75, \text{and } 1.0$ where $P = 10{,}000$ pulses with $N = 1000$ samples each. The mean power spectra of the optimized waveform sets are shown in Fig. 8, while the RMS and mean autocorrelations are illustrated in Figs. 9 and 10. Implementation of $\alpha = 0$ implies a standard FTE metric in the passband, while $\alpha = 1$ implies scaled error weighting akin to Log-FTE.

For the error weights when $\alpha = 0$, the ensuing waveform set demonstrates overall lower RMS sidelobes but higher mean sidelobes. At the other extreme when $\alpha = 1$, the waveform set demonstrates overall higher RMS sidelobes but lower mean sidelobes. Because all waveforms have finite time-bandwidth degrees-of-freedom, the allocation of said degrees must be distributed to the high-power spectral regions (causing degraded match in low-power regions) or distributed uniformly over the spectrum. High-power region match is important for smaller aggregate time-bandwidth products ($P\times TB$), while low-power region matching is important otherwise. Of interesting note, as α increases to achieve a uniform match, the minimum sinc sidelobe in the mean autocorrelation consequently decreases. When $\alpha = 0$, a degree of sinc sidelobe structure appears even in the RMS autocorrelation near the mainlobe.

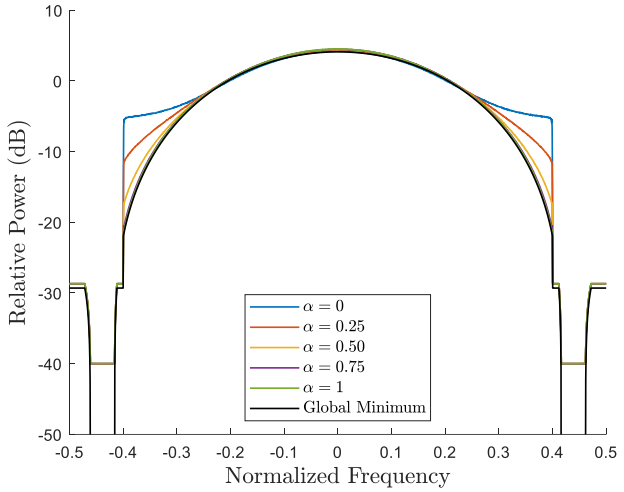

Fig. 8: Mean power spectra $\frac{1}{P}\sum_{\forall p}\left|\tilde{\mathbf{A}}\mathbf{s}_p\right|^2$ for SWiFTE with varying α; for $P = 10{,}000$ pulses, $N = 1000$ samples.

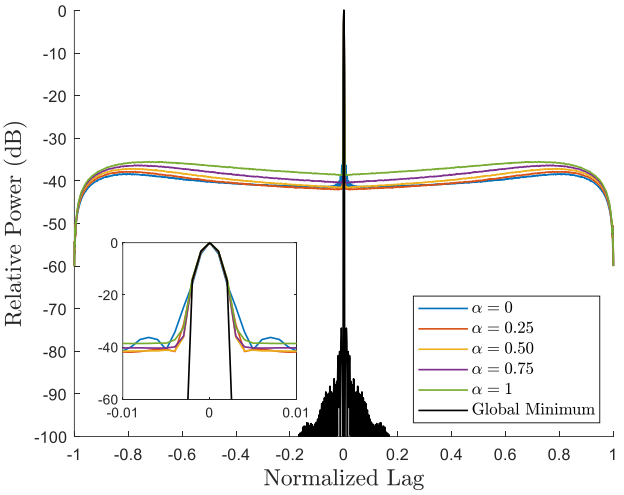

Fig. 9: RMS autocorrelation $\sqrt{\frac{1}{P}\sum_{\forall p}\left|\mathbf{r}_p\right|^2}$ for SWiFTE with varying α; for $P = 10{,}000$ pulses, $N = 1000$ samples.

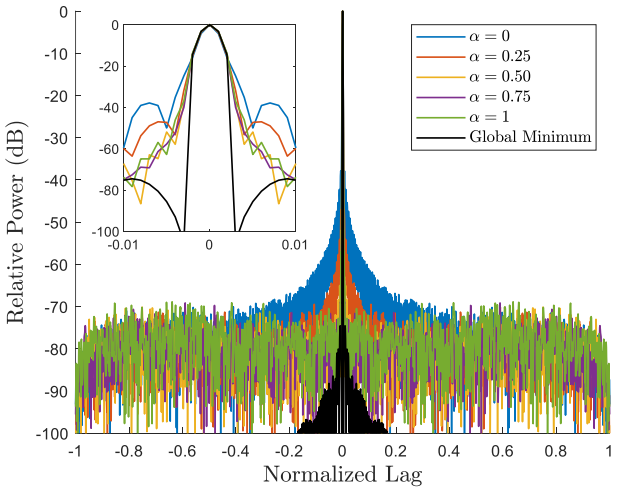

Fig. 10: Mean autocorrelation $\frac{1}{P}\sum_{\forall p}\mathbf{r}_p$ for SWiFTE with varying α; for $P = 10{,}000$ pulses, $N = 1000$ samples.

VI. Conclusions

Tradeoffs have been demonstrated between autocorrelation sidelobe level, mainlobe resolution, and spectral containment in consideration of fixed time-bandwidth degrees-of-freedom. Performance analysis of spectrally efficient RFM waveforms has revealed important design criterion via power spectrum matching. The impact of transmitter distortion on diverse waveform designs requires further analysis.

References

[1] S.D. Blunt, *et al*., "Principles and applications of random FM radar waveform design," *IEEE Aerospace & Electronic Systems Mag.*, vol. 35, no. 10, pp. 20-28, Oct. 2020.

[2] B. Ravenscroft, J.W. Owen, J. Jakabosky, S.D. Blunt, A.F. Martone, K.D. Sherbondy, "Experimental demonstration and analysis of cognitive spectrum sensing and notching for radar," *IET Radar, Sonar & Navigation,* vol 12. pp. 1466-1475.

[3] J. Owen, C. Mohr, B. Ravenscroft, S. Blunt, B. Kirk, A. Martone, "Real-time experimental demonstration and evaluation of open-air sense-and-notch radar," *IEEE Radar Conf.*, New York City, NY, Mar. 2022.

[4] C.A. Mohr, P.M. McCormick, C.A. Topliff, S.D. Blunt, J.M. Baden, "Gradient-based optimization of PCFM radar waveforms," *IEEE Trans. Aerospace & Electronic Systems*, vol. 57, no. 2, pp. 935-956, Apr. 2021.

[5] J.W. Owen, P.M. McCormick, C.C. Jones, S.D. Blunt, "On the optimality of spectrally notched radar waveform & filter designs," *IEEE Radar Conf.,* San Antonio, TX, May 2023.

[6] J. Jakabosky, S.D. Blunt, B. Himed, "Waveform design and receive processing for nonrecurrent nonlinear FMCW radar," *IEEE Intl. Radar Conf.*, Arlington, VA, May 2015.

[7] J. Jakabosky, S.D. Blunt, B. Himed, "Spectral-shape optimized FM noise radar for pulse agility," *IEEE Radar Conf.*, Philadelphia, PA, May 2016.

[8] C.A. Mohr, P.M. McCormick, S.D. Blunt, C. Mott, "Spectrally-efficient FM noise radar waveforms optimized in the logarithmic domain," *IEEE Radar Conf.*, Oklahoma City, OK, Apr. 2018.

[9] C.A. Mohr, S.D. Blunt, "FM noise waveforms optimized according to a temporal template error (TTE) metric," *IEEE Radar Conf.*, Boston, MA, Apr. 2019.

[10] C.A. Mohr, S.D. Blunt, "Designing random FM radar waveforms with compact spectrum," *IEEE Intl. Conf. Acoustics, Speech & Signal Processing*, Toronto, ON, Canada, June 2021.

[11] C.A. Mohr, J.W. Owen, S.D. Blunt,C.T. Allen, "Zero-order reconstruction optimization of waveforms (ZOROW) for modest DAC rates," *IEEE Intl. Radar Conf.*, Washington, DC, May 2020.

[12] D.C. Liu, J. Nocedal, "On the limited memory BFGS method for large scale optimization," *Mathematical Programming*, vol. 45, pp. 503-528, Aug. 1989.

[13] N. Vervliet, O. Debals, L. Sorber, M. Van Barel, L. De Lathauwer, *Tensorlab 3.0,* https://www.tensorlab.net/, Mar. 2016.

[14] C.A. Mohr, S.D. Blunt, "Analytical spectrum representation for physical waveform optimization requiring extreme fidelity," *IEEE Radar Conf.*, Boston, MA, Apr. 2019.

[15] B. White, M. Heintzelman, S.D. Blunt, "Alternative "bases" for gradient-based optimization of parameterized FM radar waveforms," *IEEE Radar Conf.*, San Antonio, TX, May 2023.

[16] S.D. Blunt, M. Cook, J. Jakabosky, J. De Graaf and E. Perrins, "Polyphase-coded FM (PCFM) radar waveforms, part I: implementation," *IEEE Trans. Aerospace & Electronic Systems*, vol. 50, no. 3, pp. 2218-2229, July 2014.

[17] J. Roberts, "Angle modulation: the theory of system assessment," *IEE Telecommunications Series*. Jan. 1977.